DOI: 10.1002/chem.200((……))

Supramolecular Recognition and Selective Protein Uptake by Peptide Hybrids

Marisa Juanes[†], Irene Lostalé-Seijo[†], Juan R. Granja[†] & Javier Montenegro[†]*

Abstract: The intracellular transport of exogenous proteins has emerged as one of the most promising methodologies for biotechnology and chemical biology. Current protein delivery is mainly approached by liposome encapsulation, translational fusion and ionic/hydrophobic non-covalent aggregation with transporting molecular vehicles. We here introduce the concept of supramolecular recognition and selective transport of proteins by peptide hybrid materials. We have designed a helical amphiphilic cationic peptide that bears two orthogonal alkoxyamines for the precise anchoring of protein ligands. After the attachment of these protein ligands, the peptide showed a high binding affinity for its protein target (i.e. mannose/Concanavalin A, Biotin/Streptavidin). The resulting peptide/protein hybrids were taken up by human cells such as HeLa and HepG2. The concept described in this manuscript could potentially be adapted, through the appropriate choice of ligands, to the transport of other proteins with suitable supramolecular binding motifs.

Keywords: Supramolecular systems · membranes · peptides · penetrating peptides · amphiphiles · protein · transport

Introduction

The selective transport of proteins across the cell membrane is a central challenge in protein therapy and chemical biology.[1-4] The emergence of protein therapeutics demands innovative methods for the intracellular delivery of exogenous antibodies, programmable enzymes and transcription factors.[5] Furthermore, expression of proteins by standard plasmid transfection or by mRNA protocols still suffers from significant limitations related with permanent recombination and/or polynucleotides instability.[6] Therefore, as biotechnology evolves, we need to develop conceptually new ways to transport and deliver proteins inside cells. Classical approaches for protein transport include liposome encapsulation, viral delivery, covalent capture, electroporation and translational fusion to penetrating tags.[2,7] Nature-inspired penetrating peptides[8-13] are among the most commonly employed tags in translational fusion.[14-19] However, protein fusion requires tedious steps of transfection, bacterial expression and purification.[2] On the other hand, non-covalent approaches are mainly based on non-specific electrostatic interactions[20] or limited to the biotin/streptavidin couple.[21] New techniques have recently been developed to achieve intracellular protein delivery.[3,5,22-25] These methodologies include polymeric tailoring,[3] dynamic nanoencapsulation,[22] target fusion to supercharged proteins[5] and hypertonic induced macropinocytosis.[23] However, none of the aforementioned examples represents a protocol for selective protein recognition and cellular internalization. The design of supramolecular vectors that could selectively recognize[26] and transport proteins across the cell membrane, without further manipulation, would represent a conceptual breakthrough towards the design of selective protein delivery vehicles. We envisaged that a hybrid membrane carrier that could integrate transport and recognition motifs would be a simple approach to tackle this challenge.

Lectins are carbohydrate-specific proteins that participate in numerous biological functions including cellular recognition and communication.[27] Reports on peptide folding for improved glycan presentation and lectin binding can be found scattered throughout the literature.[28-31] Furthermore, lectins are commonly overexpressed during tissue inflammation and cellular metastasis.[27,32] As a consequence, the delivery of exogenous lectins and their conjugates has been explored in the context of cell targeting and cancer therapy.[33-35] It has recently been demonstrated that peptide structure and helical amphiphilic segregation influence critical steps of the delivery process. [10,15,36-41] Helical polyglutamates have been developed as antimicrobial agents[42] that were subsequently adapted for nucleotide delivery.[43] Balanced polymeric glycopeptide hybrids for gene delivery[44,45] and nanocapsules for protein and lectin delivery[46,47] have been recently developed. However, efforts to equip short penetrating peptides with glycan moieties have met with limited success.[48]

We hypothesized that a short helical peptide would be ideal to adjust and orientate cationic, hydrophobic and protein ligand (i.e. glycans, biotin) units along a biomimetic scaffold with selective protein recognition and membrane translocation properties (Fig. 1A). In this peptide, the spatial distribution of charges and hydrophobicity would enhance membrane partition and uptake and, at the same time, the peptide would perform as a biocompatible scaffold for the orthogonal positioning of protein recognition units (Fig. 1B). We report here the *'de novo'* design and synthesis of these amphiphilic peptides bearing alkoxyamine connectors for the anchoring of protein ligands. After the incorporation of the ligands, the peptides bind their model proteins targets (i.e. mannose for

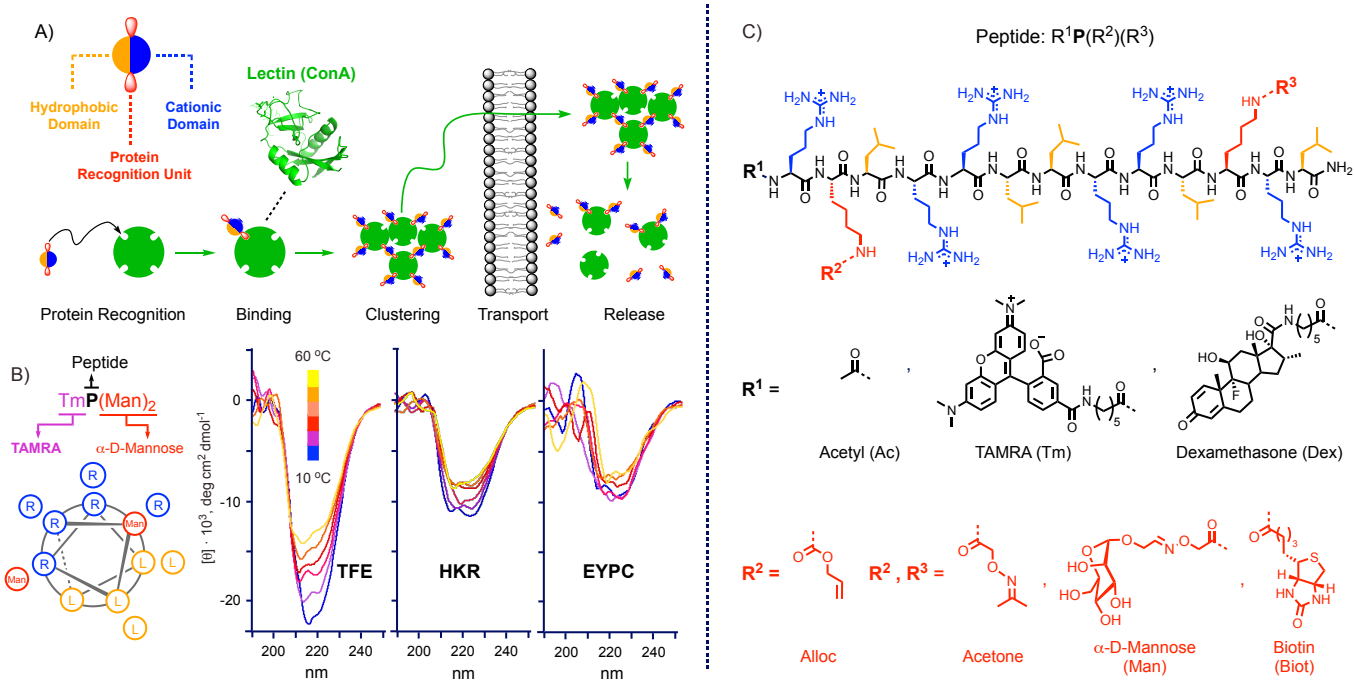

Figure 1. Peptide structure, circular dichroism and proposed model for the selective transport mechanism. **A)** Minimalist representation of the transporting peptide with amphiphilic segregated domains in blue and orange and the protein recognition units in red. Scheme of the different steps involved in selective protein intracellular delivery: recognition, binding, transport and release. B) The acronym R^1**P**(R^2)(R^3) indicates: N-terminal group R^1, peptide sequence **P** and the anchored substituents R^2 and R^3. Heptad-based wheel diagram for the helical conformation of the peptide Tm**P**$(Man)_2$ employed in the cell transport experiments. CD spectra in different conditions: TFE (trifluoroethanol), HKR buffer (pH 7.4) and Egg yolk phosphatidylcholine (EYPC) liposomes. The percentage of helicity (at 10ºC) was 26% in neutral-pH buffer, 62% in TFE and 20% in liposome. C) Peptide structure with side chains in different colours: cationic (Arg) in blue, hydrophobic (Leu) in orange and modified lysine residues (Lys-R^2 and Lys-R^3) in red. Substituents in the N-terminal R^1: acetyl (Ac), TAMRA fluorophore (Tm) and Dexamethasone analogue (Dex). Substituents in the modified lysines R^2: Alloc and R^2, R^3: Acetone, Biotin and α-D-Mannose (Man) O-(2-acetyl) oximes derivatives.

Concanavalin A and Biotin for Streptavidin). Microscopy images, fluorescence quantification, gel electrophoresis, cell viability studies and nuclear translocation studies confirmed the uptake of the peptide/protein hybrids in two different human cell lines (HeLa and HepG2). Overall, these results validated this strategy as a feasible methodology for the selectively recognition and transport of proteins with a recognisable supramolecular binding motif.

Results and Discussion

Design. Recent studies established the influence of guanidinium distribution in the delivery properties of penetrating peptides.[37,38,49] Polyproline II helical peptides penetrate cells and they only contain three aligned guanidiniums.[37,49] Additionally, arginine spatial distribution influences the delivery of helical minimal proteins.[38] Therefore, we considered the α-helix as an optimal folding motif to segregate amphiphilic domains and adjust protein recognition ligands in a fully biocompatible peptide scaffold (Fig. 1B). The peptide sequence outlined in Fig. 1 follows hydrogen-bonding patterns (i+3, i+4) with alternating cationic and hydrophobic residues (Fig. 1C). The protein-binding units were located at the interface of the hydrophilic/hydrophobic domains to minimize the impact on the secondary structure. Peptide synthesis was accomplished by a solid phase approach using orthogonal protecting groups (Fig. S1).[50,51] The key step was the selective cleavage of the methyltrityl (Mtt) groups of the two lysines. Mtt removal proceeded in weakly acidic conditions and the reactive alkoxyamines were then coupled 'on resin' for the subsequent incorporation of aldehydes or ketones (R^2, R^3). The peptide was terminated with either a fluorophore (TAMRA), the steroid dexamethasone or by simple acetylation (R^1, Fig. 1C). Full deprotection and cleavage from the solid support was accomplished by TFA treatment and, after precipitation and washings, the peptide was re-dissolved in water and fused to the protein ligands (**R^2**, **R^3**) by a short incubation with the mannosyl aldehyde (5 minutes, quantitative, Fig. S2).[52] After HPLC purification the peptide was characterized by circular dichroism (CD) in three different solvents: trifluoroethanol (TFE), HKR buffer (pH 7.4) and liposomes. The CD of peptide Tm**P**$(Man)_2$ (where: Tm = TAMRA and Man = α-D-Mannose ligand, Fig. 1B) showed the typical bands of the α-helix. This short peptide exhibited certain helical behavior in aqueous buffer and in lipid bilayers even at high temperatures (60 ºC), although the intensity of the exciton couplings diminished (Fig. 1B).

Binding studies with a model protein Concanavalin A (ConA). We initially employed fluorescence anisotropy[53,54] to study the binding of the peptide bearing mannose ligands with its model protein target (ConA). ConA is a homotetrameric plant lectin that presents four saccharide-binding sites that recognises with specific affinity α-D-glucose and α-D-mannose residues.[55-57] Incubation of the fluorescently-labelled glycopeptides with increasing amounts of native ConA resulted in a gradual increase of the anisotropy, which indicates the formation of a higher molecular weight complex with the protein host (Fig. 2A).[54] Initial control experiments with fluorescently labelled methyl α-D-mannopyranoside and fitting to a 1:1 binding model allowed the estimation of a K_d of 137 ± 29 μM, which is consistent reported values (K_d ~ 100 μM).[31,53] The peptide Tm**P**$(Man)_2$, which contains two orthogonal mannoses, showed the maximum net anisotropy value and the best equilibrium dissociation constant (K_d = 14 ± 1 μM), which was about one order of magnitude higher than that of the mannoside control (Fig. 2A).

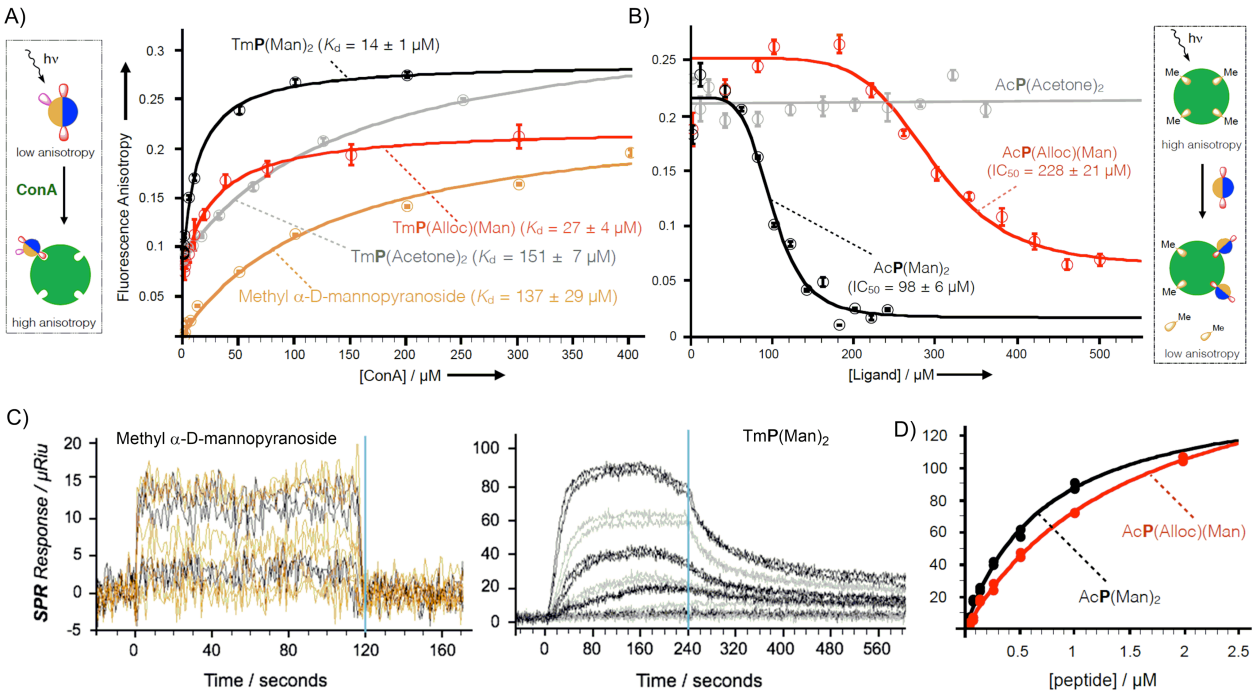

Figure 2. **Studies of peptide binding with the protein ConA**. A) Fluorescence anisotropy titrations and best fitting to a simple 1:1 binding model of fluorescent ligands (Initial peptide concentration = 100 nM) with increasing amounts of ConA in HKR buffer (pH 7.4) at 22 ºC. B) Competition experiments on ConA saturated with fluorescently labelled mannose followed by the stepwise addition of unlabelled peptides. C) Sensorgrams of the interaction of ConA (9668 μRiU) in the concentration range [Methyl a-D-mannopyranoside] = 125-1600 μM (orange/black) and [Ac**P**(Man)$_2$] = 7-1000 nM (black/gray). D) Best fitting to a simple 1:1 binding model of the steady-state SPR response for the two peptides bearing mannose recognition units. Color code for fitting graphs (A, B, D): black for peptide with two mannoses (Tm**P**(Man)$_2$), red for peptide with one mannose (Tm**P**(Alloc)(Man)), grey for peptide capped with two acetones (Tm**P**(Acetone)$_2$) and orange for methyl α-D-mannopyranoside control. In the SPR traces graph, the exact point where the ligand flow was stopped is indicated with a blue line.

The role of the mannose for protein binding was confirmed by removal of the glycans. Accordingly, the acetone capped peptide (Tm**P**(Acetone)$_2$) showed a drop in the binding affinity (K_d = 151 ± 7 μM). However, the peptide with only one mannose residue, Tm**P**(Alloc)(Man), also showed a similar affinity enhancement (K_d = 27 ± 4 μM) compared to methyl α-D-mannopyranoside.

Competition experiments were carried out to gain further insights into the stability and specificity of these peptide/protein complexes (Fig. 2B). For this purpose, ConA was initially saturated with a fluorescently labelled α-D-mannopyranoside. The resulting complex was titrated with the competitor that displaced the ligand from its binding site (Fig. 2B).[31] As expected, the peptide with the two orthogonal mannoses was the best competitor. This peptide was able to remove practically all of the labelled mannoside at the lowest concentration (IC_{50} = 98 ± 6 μM). The control peptide with only one mannose was less efficient and required more than double the concentration to remove only part of the fluorescent mannopyranoside (IC_{50} = 228 ± 21 μM). The peptide capped with acetone was not able to displace the mannopyranoside ligand (Fig. 2B). Surface plasmon resonance (SPR) was employed to further confirm this enhancement in binding affinity. The two glycopeptides and the methyl α-D-mannopyranoside were flown, at different concentrations, over a gold chip biosensor modified by immobilized Concanavalin A (Fig. 2C and S3, see methods). The sensorgram for the methylmannoside showed an abrupt increase in the resonance at time zero and this was followed by an immediate decrease in the signal as soon as the analyte stopped flowing (Fig. 2C). The SPR profile of the glycopeptide was more complex and when the ligand flow was stopped (at t = 240 s), the SPR response decreased smoothly and did not recover to the initial level. This profile indicated hindered peptide dissociation under pure buffer flow. Fitting of the steady state response to a 1:1 equilibrium model allowed the estimation of a dissociation constant for the control methyl mannoside of 97 ± 12 μM, which is in good agreement with recent reports.[58] The SPR K_d constants obtained for the glycopeptides (Ac**P**(Man)$_2$ = 0.7 ± 0.1 μM, Ac**P**(Alloc)(Man) = 1.5 ± 0.1 μM) again showed a large increase in the binding affinity (Fig. 2D). Taken together, the results obtained by the two techniques confirmed the importance of the mannose residues for protein specific recognition. The binding affinity of the peptide with a single mannose ligand, Tm**P**(Alloc)(Man) (K_d = 27 ± 4 μM), was higher than that of the methyl α-D-mannopyranoside (K_d = 137 ± 29 μM). This observation suggested that the peptide is playing a synergic and probably unspecific role together with the glycan moiety in the stabilization of the final peptide/protein complex.

Selective recognition and uptake. We next evaluated the potential uptake of the protein in HeLa cells (Fig. 3). ConA is commonly employed as a cell membrane marker due to its aggregation at the cellular membrane glycocalyx (Fig. 3K, 3L).[59] A simple cell transport experiment was performed by pre-incubation of the protein with different peptides followed by cellular incubation, buffer washing and fluorescence microscopy analysis (Fig. 3). An initial control experiment was performed with a prototypical penetrating peptide such as octaarginine. As expected, CFArg$_8$ (CF stands for carboxyfluorescein and Arg$_8$ for octaarginine, see Fig. S10) was internalized inside the cells while ConA (labelled with Alexa Fluor-647) remained at the cell membrane (Figs. 3D, 3E). However, when the transport experiment was repeated with the amphiphilic peptide bearing two mannose ligands Tm**P**(Man)$_2$, the protein was aggregated with the glycopeptide and cellular uptake was observed (Figs. 3I, 3J). Quantification of the peptide and protein co-localization gave good values (~ 0.6) for the Manders coefficients (Table S1).[60]

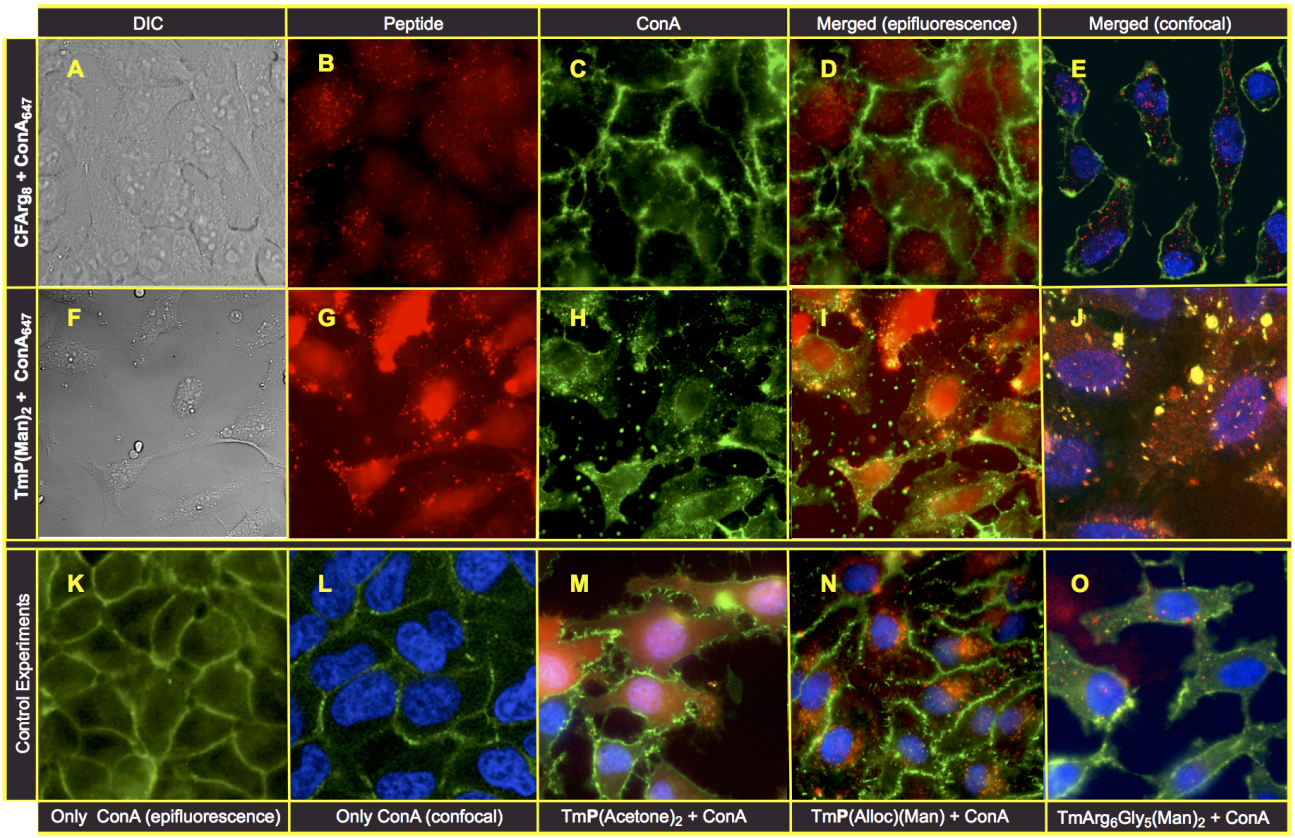

Figure 3. Selective recognition and delivery of ConA in cells. The first row (A-E) shows a series of microscopy images of the control peptide $CFArg_8$ (carboxyfluorescein conjugate) (4 μM) combined with fluorescent $ConA_{647}$ (Alexa Fluor-647). The second row (F-G) shows the analogous experiment but with the glycopeptide Tm**P**$(Man)_2$ (3 μM) and $ConA_{647}$. A) and F) Differential interference contrast (DIC) images. B) and G) epifluorescence peptide channel showing that both peptides were internalized. C) and H) epifluorescence protein channel: C) ConA remained in the membrane when incubated with octaarginine, H) ConA was internalized when incubated with the glycopeptide Tm**P**$(Man)_2$. D) and I) Epifluorescence merge channels. E) and J) CLSM merge channels. CLSM images were stained with Hoechst for nuclear visualization. ConA was $ConA_{FITC}$ (fluorescein conjugate). K) and L) Epifluorescence and CLSM (with blue nuclei) of $ConA_{FITC}$ incubated with HeLa cells. M) Epifluorescence image of HeLa cells incubated with Tm**P**$(Acetone)_2$ (2 μM) and $ConA_{FITC}$. N) Epifluorescence image of HeLa cells incubated with Tm**P**(Alloc)(Man) and $ConA_{FITC}$. O) Epifluorescence images of HeLa cells incubated with $TmArg_6Gly_5(Man)_2$ non-helical control peptide and $ConA_{FITC}$. Note that in B, C, D, E, H and I the $ConA_{647}$ and the $CFArg_8$ have been assigned to green and red channels for clarity of comparison. In all cases the concentration of fluorescent ConA was 30 nM and it was incubated with the HeLa cells for 30 min at 37 °C in HKR buffer.

As expected, the peptide without mannoses, Tm**P**$(Acetone)_2$, did not complex or transport ConA (Fig. 3M). Similarly, the peptide bearing a single mannose ligand, Tm**P**(Alloc)(Man), was unable to translocate the protein (Fig. 3N). To demonstrate that lectin binding and clustering was not sufficient for protein transport, we carried out control experiments with two different non-helical peptides with the same number of arginines ($TmArg_6Gly_5(Man)_2$ and $TmArg_6(Man)_2$) and a short cationic peptide ($TmArg_2(Man)_2$), all of them bearing two mannose residues (Figs. 3O and S4-S6). The epifluorescence images once again confirmed that the ConA could not go beyond the cell membrane. Viability studies of the peptide and the peptide/lectin complexes were carried out by the colorimetric MTT and the propidium iodide exclusion assays (Figs. S7 and S8). Both assays confirmed that the peptide alone had low toxicity at the concentrations that were employed in protein transport experiments (1 to 5 μM). However, viability studies in the presence of peptide at a fixed non-toxic concentration (5 μM) and increasing amounts of protein (ConA), showed a clear dose-response toxicity effect that was much higher than that for the peptide and the protein alone (Figs. S7 and S8). This observation constitutes further proof for the protein delivery, as ConA receptor-mediated delivery has been applied in cytotoxic cancer targeting.[33,35]

Internalization mechanism. To study the internalization mechanism, the uptake was studied in the presence of endocytic inhibitors after cell trypsinization to remove membrane bound peptides (Fig. 4).[61] Inhibition of energy-dependent pathways at 4 ºC revealed that around half of the peptide was able to translocate the cell membrane (Fig. 4C). In general different inhibitors showed a moderate or a medium reduction of the uptake suggesting a combination of different endocytic mechanisms operating at the same time. The Lysotracker™ assay showed that peptide/protein complexes did not co-localize within the lysosomes (Fig. 4B). The internalization was also monitored in a fluorescence time-lapse video (Video S1, see supporting information). Intriguingly, the punctate fluorescence signal observed in the cytosol became increasingly diffuse and intense with time (~ 1 hour, video S1). To further study the cytosolic distribution of the peptide alone or in combination with the protein, a glucocorticoid-induced GFP-translocation assay was employed (Fig. 4A, 4D and Fig. S9).[38] In this assay cells are transfected with a plasmid to express GFP (green fluorescent protein) fused to the ligand-binding domain of the glucocorticoid receptor (GR). This receptor is expressed and confined at the cytosol and, upon binding to dexamethasone, it undergoes a conformational change that triggers its nuclear accumulation.[62] Thus, the nuclear distribution of GR-GFP (translocation ratio) is an indicator of the earlier cytosolic presence of the dexamethasone-labelled peptide (Fig. S9). Incubation of cells with Dex**P**$(Man)_2$, both in the absence (red column) and presence of ConA (green column), caused a significant increase in the translocation ratio, which indicates that the dexamethasone labelled peptide is reaching the cytosol (Fig. 4D).

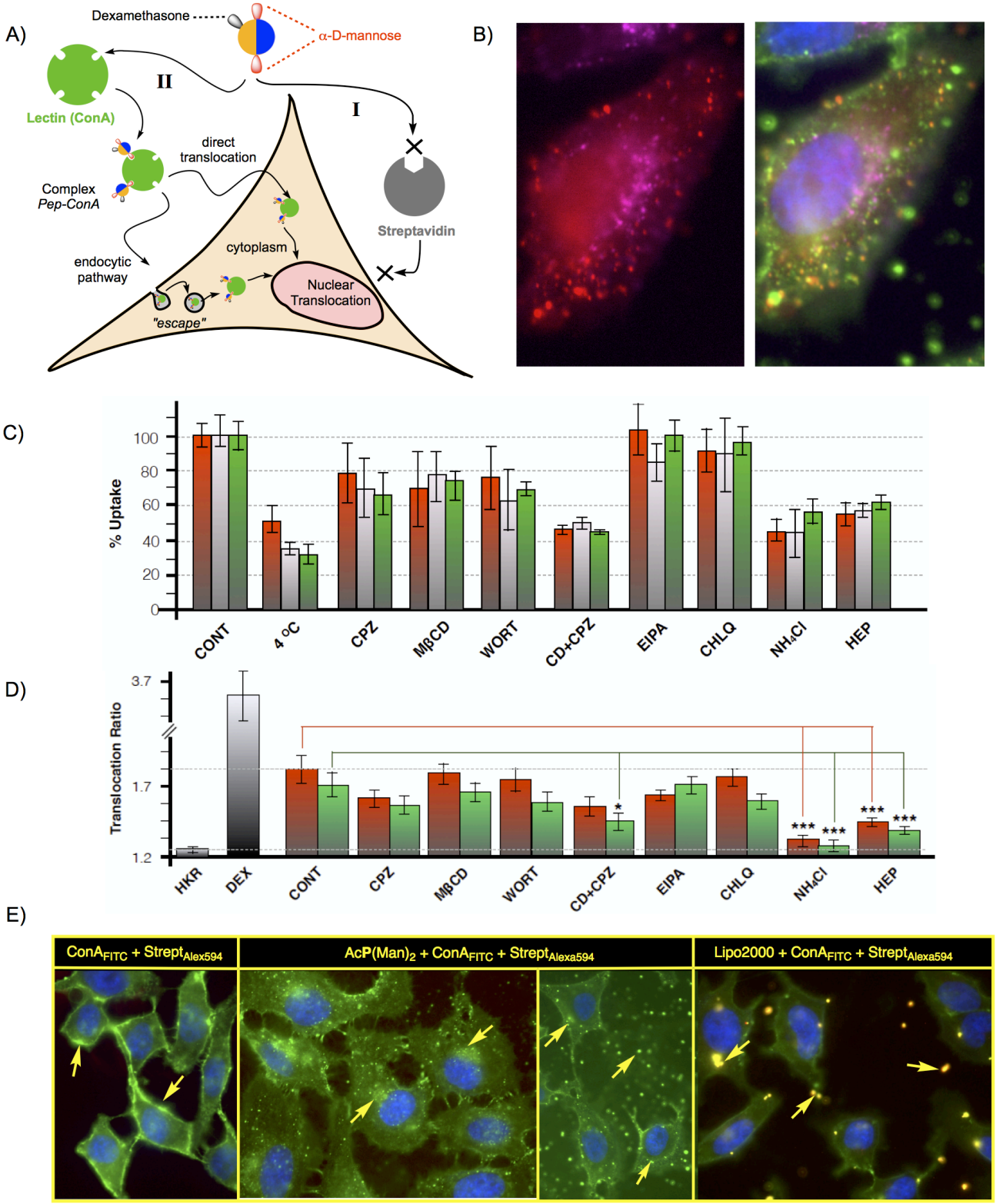

Figure 4 | Internalization mechanism and selective protein transport. A) General scheme: I) *Discriminatory recognition* of ConA in the presence of Streptavidin. II) *Translocation assay*: GR-GFP fused protein is expressed in the pale orange cytoplasm (GFP: green fluorescent protein, GR: glucocorticoid receptor). Cytosolic delivery of the peptide incorporating a dexamethasone ligand triggers GR-GFP conformational changes, exposure of NLSs and nuclear translocation of GR-GFP. B) *Lysotracker™ assay* (see methods): peptide is in red, Lysotracker™ is in magenta and protein is in green. C) *Endocytic inhibition* of the uptake (see supporting information). In the histogram the columns are in red for peptide alone, in grey for the peptide/protein complex (following the fluorescence of the labelled peptide Tm**P**$(Man)_2$) and in green (following the fluorescence of labelled protein $ConA_{FITC}$). Cont: control; CPZ: chlorpromazine; MβCD: methyl-β-cyclodextrin; WORT: Wortmannin; CD+CPZ: Combination of MβCD and CPZ; CHLQ: chloroquine; HEP: heparin. Error bars indicate SD of three replicates. D) *GR-GFP translocation ratios*. Translocation ratios columns are in red for the peptide Dex**P**$(Man)_2$ and in green for the peptide/protein complex. HKR stands for the control experiment with buffer. DEX stands for the control experiment with neat dexamethasone. Ratios obtained from the analysis of 40 to 80 cells from 20 to 30 images and calculated with CellProfiler. Error bars indicate SE. The asterisk (*) indicates a significant value with $p \leq 0.05$ and (***) $p \leq 0.001$ in a two-tailed t-test with Bonferroni correction. E) *Discriminatory recognition and transport of ConA*. HeLa cells incubated with a mixture of 30 nM of $ConA_{FITC}$ (green), 30 nM of $Streptavidin_{594}$ (Alexa Fluor-594, red) and with the unlabelled peptide (4 μM) or Lipofectamine 2000. Yellow arrows indicate: membrane-labelling by ConA (mixture of proteins), selective internalization of ConA near the nuclei and peptide/protein aggregates (unlabelled peptide) and non-selective aggregates of the two proteins (Lipofectamine 2000)

Interestingly, nuclear translocation experiments in the presence of clathrin and caveolae inhibitors led to a significant decrease of the translocation ratio. This result suggests that the fraction of peptide, or its protein complex, that is internalized by clathrin and caveolae receptors, is able to escape from these particular endocytic pathways. Finally, to confirm the presence of the lectin in the cytosol, the ConA was conjugated with the dexamethasone corticoid (Fig. 5A, see supporting information). Transport experiments confirmed the higher nuclear translocation and thus cytosolic presence of the ConA for the peptide vector in comparison with control experiments in the absence of peptide or in the presence of the Lipofectamine 2000 vector (Fig. 5A).

Selective transport and scope. In order to demonstrate protein discrimination, transport experiments with $ConA_{FITC}$ were carried out in the presence of a second labelled protein, namely $Streptavidin_{594}$ (Alexa Fluor-594). As expected, the peptide was complexed the ConA and the peptide/protein aggregates did only contain the lectin (Fig. 4E). We performed analogous control transport experiments with a commercially available nano-vehicle, Lipofectamine 2000, which is known to be a suitable excellent vehicle for different proteins.[5] These experiments showed that the Lipofectamine transported the ConA and the Streptavidin without selectivity (Figs. 4E and S12). We could confirm the presence of yellow dots of protein aggregates that were composed of Streptavidin (red) and ConA (green).

To confirm the integrity of the cargo, gel electrophoresis was carried out for cellular extracts after internalization experiments and extensive cell washing and trypsinization (Fig. S13). The gels showed no degradation bands confirming the presence of intact protein (Fig. S13). The peptide/protein concentration ratio at the incubation step had an impact on the complexes size and uptake (Fig. S14). AFM measurements were carried out to investigate the sizes of peptide protein clusters (Fig. S15). The AFM micrographs confirmed the presence of aggregates of different sizes. However, due to the high polydispersity of these aggregates, the correlation of their sizes with the uptake efficiency was proven challenging (Fig. S15).

We next exchanged the glycan unit for a biotin ligand to explore the extension of the methodology to different proteins (Fig. 1C, Fig. S11). Incubation of the biotinylated peptide (Ac**P**$(Biot)_2$) with fluorescently labelled Streptavidin and subsequent cell transport experiments confirmed the presence of internalized Streptavidin as shown in the fluorescence confocal micrographs (Fig. 5B). Finally, protein transport experiments in HepG2 cells were performed to explore the extension of the method to different cell lines. These transport experiments, in a different cell line, showed similar results as the previously observed with HeLa cells. In this case, the protein targets (ConA and Streptavidin) were incubated with HepG2 cells in the presence (or absence) of the acetylated peptides bearing the corresponding mannose and biotin ligands. The micrographs of the cells confirmed the presence of internalized fluorescent proteins when the peptide vehicle was present (Fig. 5C and 5D). On the other hand, in the absence of peptides, the pictures showed the membrane localization of the ConA or the total lack of protein signal for the Streptavidin.

Discussion

The objective of this study was to introduce the supramolecular recognition and the selective uptake of proteins. For this purpose we have designed an amphiphilic peptide that displayed orthogonal dynamic connectors[8] for protein ligand anchoring. Two assays (SPR and fluorescence anisotropy) confirmed the increased affinity of the peptide bearing two mannoses for its host protein (Con A). The enhanced affinity observed for the peptide with a single glycan unit compared with the methylmannoside suggested a potential unspecific synergic interaction between the peptide and the protein. Electrostatic interactions between the cationic peptide and ConA, a protein with a net negative charge,[63] could be involved in the stabilization of the peptide/protein complex. The good fitting of the anisotropy data and the plateau observed for the surface plasmon resonance response, supported a fitting to 1:1 binding model. Furthermore, the experimental observation that the K_d value obtained for the peptide with two mannoses was approximately half the value for the peptide with one mannose (Tm**P**$(Man)_2$: $K_d = 14 \pm 1$ μM *vs* Tm**P**(Alloc)(Man): $K_d = 27 \pm 4$ μM) suggested that there was no cooperativity involved. Peptide helicity did not dramatically increase the binding affinity with the protein (Table S2). However, the helicity did increase the structural order of the peptide/protein complex as observed by fluorescence anisotropy. Substitution at the N-terminal with either a fluorophore or an acetyl group did not have strong influence in the binding and/or in the cell internalization (Figs. 2, 3 and 4E). Different endocytic inhibitors showed a slight (~ 20%) decrease in total uptake, suggesting that different internalization mechanisms could be operating at the same time.[64] The nuclear translocation assay confirmed that the peptide and the protein were able to reach the cell cytosol. The results reported here constitute a proof of concept for protein selective recognition and delivery. However, performing these experiments in complex biological media can be challenging as for instance, the presence of glucose and serum proteins can block recognition and hinder uptake. Although, we could perform the protein selective uptake experiments in two cell lines (HeLa and HepG2), the different glycosylation pattern and metabolic rate of other different cells might have a strong influence on the endocytic uptake of these and other lectins. However, the presence of a penetrating peptide counterpart that could assist in the endosomal escape will certainly enhance the presence of the cytosolic levels of the proteins transported.

Conclusions

In this work we have introduced the concept of supramolecular recognition and uptake of proteins across the cell membrane by biomimetic peptide materials. We have applied this concept to the selective uptake of ConA and Streptavidin in two different cell lines such as HeLa and HepG2 cells. Microscopy images, fluorometry quantification, cell viability and nuclear translocation experiments confirmed the selective recognition and delivery of two protein targets in two different cell lines. We believe that this strategy could be adapted, through an informed choice of ligands, to other proteins with a recognisable supramolecular binding motif. In this regard, the peptide scaffold described here will allow the conjugation of different ligands and reducing glycans through its nucleophilic linkers. These hybrid biomaterials and this methodology could find applications in protein therapeutics and drug targeting.

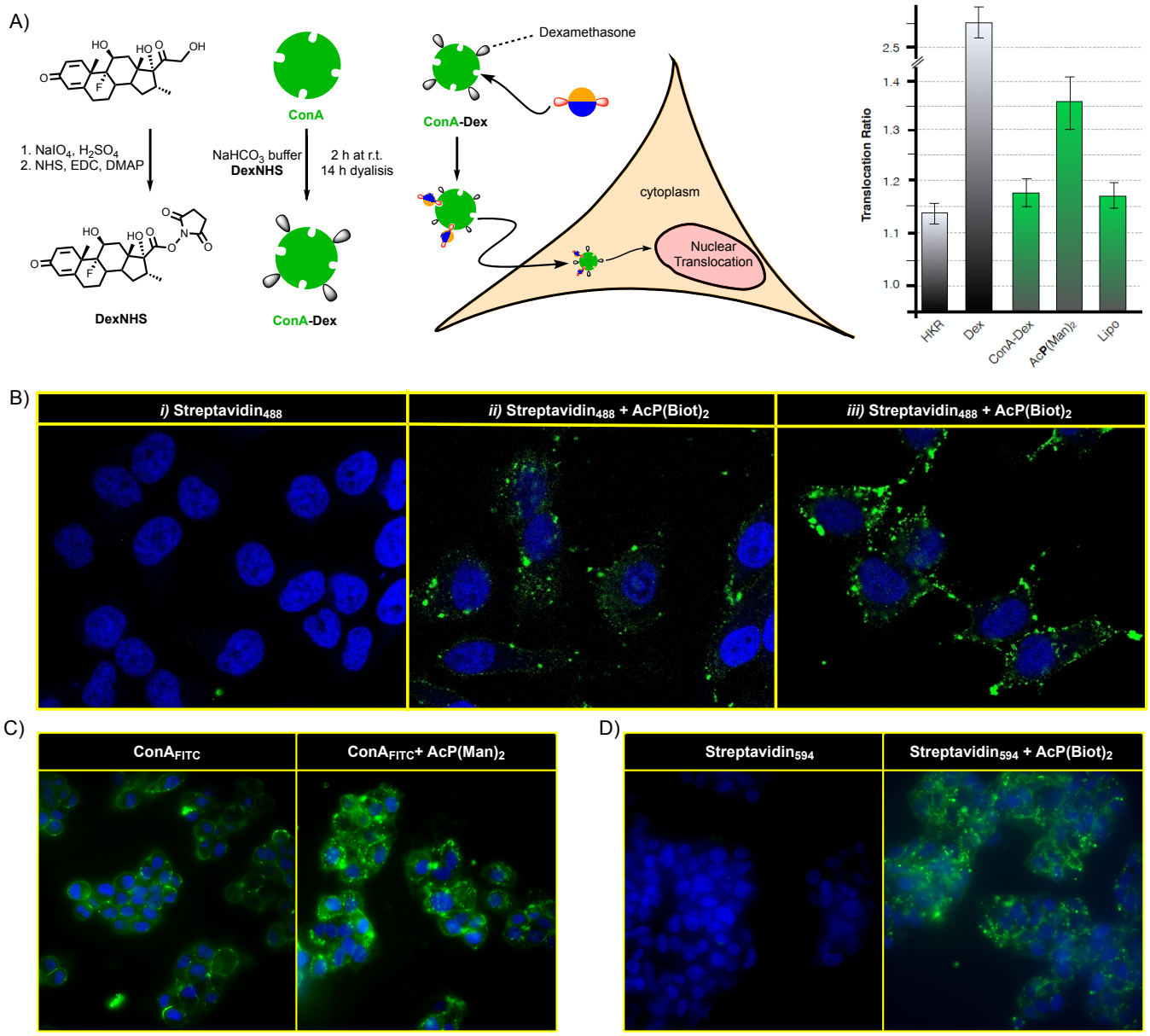

Figure 5 | Cytosolic presence and extension to Streptavidin. A) Cytosolic presence of ConA. Schemes for activation of dexamethasone, ConA labelling and transport experiment are shown on the left. Nuclear translocation ratio for dexamethasone labelled ConA: buffer (HKR), dexamethasone (Dex), dexamethasone labelled protein (ConA-Dex), acetylated di-mannosyl peptide combined with ConA-Dex (Ac**P**(Man)$_2$) and Lipofectamine 2000 combined with ConA-Dex (Lipo). B) CLSM images of HeLa cells incubated with Streptavidin$_{488}$ in the absence i) or presence ii) and iii) of the peptide Ac**P**(Biot)$_2$. The concentration of [Streptavidin$_{488}$] was 5 μM in *i)*, 3 μM in *ii)* and 5 μM in *iii)*. The peptide [Ac**P**(Biot)$_2$] concentration was 4 μM. C) ConA transport in HepG2 cells. HepG2 cells were incubated with 30 nM ConA$_{FITC}$ (green) in the presence or not of 3 μM of Ac**P**(Man)$_2$. D) Streptavidin transport in HepG2 cells. HepG2 cells were incubated with 3 μM Streptavidin$_{594}$ in the presence or absence of 4 μM Ac**P**(Biot)$_2$.

Methods

Full experimental details for peptide synthesis, circular dichroism, fluorescence assays, surface plasmon resonance, cellular uptake, inhibition experiments and nuclear translocation assays can be found in the supporting information.

Peptide synthesis. All peptides were synthesized by manual Fmoc solid-phase peptide synthesis using Rink Amide resin. Full details of the synthesis can be found in the supporting info. The characterization was performed by analytical HPLC, ^{1}H NMR spectroscopy, and low and high-resolution mass spectrometry.

Fluorescence anisotropy. Fluorescence anisotropy measurements were carried out at 20 °C in a quartz cell of 1 cm path length at a final volume of 0.6 mL using the following settings: integration time: 1.0 s; excitation slit width: 3.0 nm; emission slit width: 3.0 nm; excitation wavelength 559 nm; emission wavelength 585 nm. ConA was dissolved in 0.1 M HEPES buffer, pH 7.4, containing 0.9 M NaCl, 1 mM $MnCl_2$ and 1 mM $CaCl_2$, which were added to the solution containing 100 nM ligand (Tm-peptides) in 0.1 M HEPES buffer, pH 7.4, containing 1 mM $MnCl_2$, 1 mM $CaCl_2$, 0.9 M NaCl and varying the lectin (ConA) concentration from 1 to 300 μM. Competition titration experiments were performed using 150 μM Concanavalin A in 0.1 M HEPES buffer (pH 7.4) containing 1 mM $MnCl_2$, 1 mM $CaCl_2$, 0.9 M NaCl, 160 nM 4-methylumbelliferyl α-D-mannopyranoside (excitation wavelength 355 nm; emission wavelength 460 nm) and varying the unlabelled peptides concentration from 10 to 300 μM. The data was fitted to a 1:1 equilibrium model to evaluate the K_d.

Surface plasmon resonance. ConA was immobilized in one vertical channel of a GLH chip in HEPES buffer (10 mM HEPES, 150 mM NaCl, 1 mM $CaCl_2$, 1 mM $MgCl_2$ and 0.005% Tween 20, pH 7.4) at 25 ºC. Two channels of the chip were activated for 300 s, at a flow rate 30 μL/min, using a mixture of 40 mM EDC and 10 mM sulfo-NHS. This was followed by an injection of 300 μL of ConA, at 30 μg/mL, in 10 mM acetate buffer (pH 4.0) in the first channel, and in the second channel 10 mM acetate buffer was used as reference. Finally, 1 M ethanolamine-HCl (pH 8.5) was injected, at a flow rate of 30 μL/min, for 300 s to deactivate any remaining activated

carboxyl groups. This resulted in the immobilization of 9668 RU of ConA. The chip was then rotated by 90° and buffer injections were performed until a stable signal was achieved (for at least 30 min). The Methyl α-D-mannopyranoside was applied at a flow rate of 50 µL/min for 120 s in the association phase, which was followed by a 180 s dissociation phase. The two peptides were applied at a flow rate of 50 µL/min for 240 s in the association phase, which was followed by a 180 s dissociation phase. The steady state response was fitted to a 1:1 equilibrium model to evaluate the K_d.

Cell transport experiments. HeLa cells growing on four chamber glass bottom dishes were washed with HEPES–Krebs–Ringer (HKR) buffer (5 mM HEPES, 137 mM NaCl, 2.68 mM KCl, 2.05 mM $MgCl_2$, 1.8 mM $CaCl_2$, pH 7.4) and nuclei were stained by incubation with 1 µM Hoechst 33342 in HKR for 30 min. The peptide and protein were diluted in HKR and incubated for 7 min at room temperature to allow the formation of the complexes. Cells were washed with HKR and incubated with the complexes for another 30 min. Cells were washed again to remove excess peptide before performing epifluorescence microscopy using a Nikon Eclipse Ti-E inverted microscope or confocal microscopy with a Leica SP5 microscope. For lysosomal staining, cells were further incubated for 15 min with 100 nM Lysotracker Green DND-26 before imaging. Images were analyzed with ImageJ and the co-localization parameters (Manders coefficients) were calculated using the Coloc2 plugin selecting the Costes method of threshold regression (Table S1).

References

[1] B. Leader, Q. J. Baca, D. E. Golan, *Nat. Rev. Drug. Discov.* **2008**, *7*, 21–39.

[2] A. Muñoz Alarcón, H. Helmfors, K. Karlsson, Ü. Langel, *Fusion Protein Technologies for Biopharmaceuticals: Applications and Challenges* **2013**, 397–411.

[3] G. Fuhrmann, A. Grotzky, R. Lukic, S. Matoori, P. Luciani, H. Yu, B. Zhang, P. Walde, A. D. Schluter, M. A. Gauthier, et al., *Nat. Chem.* **2013**, *5*, 582–589.

[4] S. Mitragotri, P. A. Burke, R. Langer, *Nat. Rev. Drug. Discov.* **2014**, *13*, 655–672.

[5] J. A. Zuris, D. B. Thompson, Y. Shu, J. P. Guilinger, J. L. Bessen, J. H. Hu, M. L. Maeder, J. K. Joung, Z.-Y. Chen, D. R. Liu, *Nat. Biotechnol.* **2015**, *33*, 73–80.

[6] M. A. Kay, *Nat. Rev. Genet.* **2011**, *12*, 316–328.

[7] Z. Gu, A. Biswas, M. Zhao, Y. Tang, *Chem. Soc. Rev.* **2011**, *40*, 3638–3655.

[8] J. M. Priegue, D. N. Crisan, J. Martínez-Costas, J. R. Granja, F. Fernandez-Trillo, J. Montenegro, *Angew. Chem. Int. Ed.* **2016**, *55*, 7492–7495.

[9] I. Louzao, R. García-Fandiño, J. Montenegro, *J. Mat. Chem. B* **2017**, *5*, 4426–4434.

[10] M. Pazo, H. Fernández-Caro, J. M. Priegue, I. Lostalé-Seijo, J. Montenegro, *Synlett* **2017**, *28*, 924–928.

[11] J. Montenegro, S. Matile, *Chem. Asian J.* **2011**, *6*, 681–689.

[12] C. Gehin, J. Montenegro, E.-K. Bang, A. Cajaraville, S. Takayama, H. Hirose, S. Futaki, S. Matile, H. Riezman, *J. Am. Chem. Soc.* **2013**, *135*, 9295–9298.

[13] A. Fuertes, J. Marisa, J. R. Granja, J. Montenegro, *Chem. Commun.* **2017**, *53*, 7861–7871.

[14] R. Fischer, M. Fotin-Mleczek, H. Hufnagel, R. Brock, *ChemBioChem,* **2005**, *6*, 2126–2142.

[15] P. M. Fischer, *Med. Res. Rev.* **2007**, *27*, 755–795.

[16] I. Nakase, T. Takeuchi, S. Futaki, *Methods Mol. Biol.* **2015**, *1324*, 387–396.

[17] J. M. Hyman, E. I. Geihe, B. M. Trantow, B. Parvin, P. A. Wender, *Proc. Natl. Acad. Sci. U. S. A.* **2012**, *109*, 13225–13230.

[18] E. G. Stanzl, B. M. Trantow, J. R. Vargas, P. A. Wender, *Acc. Chem. Res.* **2013**, *46*, 2944–2954.

[19] H. D. Herce, D. Schumacher, A. F. L. Schneider, A. K. Ludwig, F. A. Mann, M. Fillies, M.-A. Kasper, S. Reinke, E. Krause, H. Leonhardt, et al., *Nat. Chem.* **2017**, *9*, 762–771.

[20] M. C. Morris, J. Depollier, J. Mery, F. Heitz, G. Divita, *Nat. Biotechnol.* **2001**, *19*, 1173–1176.

[21] G. Gasparini, S. Matile, *Chem. Commun.* **2015**, *51*, 17160–17162.

[22] M. Yan, J. Du, Z. Gu, M. Liang, Y. Hu, W. Zhang, S. Priceman, L. Wu, Z. H. Zhou, Z. Liu, et al., *Nat. Nanotech.* **2010**, *5*, 48–53.

[23] D. S. D'Astolfo, R. J. Pagliero, A. Pras, W. R. Karthaus, H. Clevers, V. Prasad, R. J. Lebbink, H. Rehmann, N. Geijsen, *Cell* **2015**, *161*, 674–690.

[24] K. A. Andersen, T. P. Smith, J. E. Lomax, R. T. Raines, *Acs Chem. Biol.* **2016**, *11*, 319–323.

[25] K. A. Mix, J. E. Lomax, R. T. Raines, *J. Am. Chem. Soc.* **2017**, *139*, 14396–14398.

[26] C. S. Mahon, D. A. Fulton, *Nat. Chem.* **2014**, *6*, 665–672.

[27] H. Lis, N. Sharon, *Chem. Rev.* **1998**, *98*, 637–674.

[28] G. L. Simpson, A. H. Gordon, D. M. Lindsay, N. Promsawan, M. P. Crump, K. Mulholland, B. R. Hayter, T. Gallagher, *J. Am. Chem. Soc.* **2006**, *128*, 10638–10639.

[29] A. S. Norgren, M. Geitmann, U. H. Danielson, P. I. Arvidsson, *J. Mol. Recognit.* **2007**, *20*, 132–138.

[30] T. M. Altamore, C. Fernández-García, A. H. Gordon, T. Hübscher, N. Promsawan, M. G. Ryadnov, A. J. Doig, D. N. Woolfson, T. Gallagher, *Angew. Chem. Int. Ed.* **2011**, *50*, 11167–11171.

[31] N. J. Pawar, U. Diederichsen, D. D. Dhavale, *Org. Biomol. Chem.* **2015**, *13*, 11278–11285.

[32] N. Yamazaki, S. Kojima, N. V. Bovin, S. André, S. Gabius, H. J. Gabius, *Adv. Drug. Deliv. Rev.* **2000**, *43*, 225–244.

[33] A. Amin, M. L. Oo, T. Senga, N. Suzuki, G. S. Feng, M. Hamaguchi, *Cancer Res.* **2003**, *63*, 6334–6339.

[34] F. Gabor, E. Bogner, A. Weissenboeck, M. Wirth, *Adv. Drug. Deliv. Rev.* **2004**, *56*, 459–480.

[35] S.-H. Park, Y. P. Choi, J. Park, A. Share, O. Francesconi, C. Nativi, W. Namkung, J. L. Sessler, S. Roelens, I. Shin, *Chem. Sci.* **2015**, *6*, 7284–7292.

[36] M. Magzoub, L. E. G. Eriksson, A. Gräslund, *Biochim. Biophys. Acta* **2002**, *1563*, 53–63.

[37] D. S. Daniels, A. Schepartz, *J. Am. Chem. Soc.* **2007**, *129*, 14578–14579.

[38] J. S. Appelbaum, J. R. La Rochelle, B. A. Smith, D. M. Balkin, J. M. Holub, A. Schepartz, *Chem. Biol.* **2012**, *19*, 819–830.

[39] G. Gasparini, E.-K. Bang, J. Montenegro, S. Matile, *Chem. Commun.* **2015**, *51*, 10389–10402.

[40] I. Lostalé-Seijo, I. Louzao, M. Juanes, J. Montenegro, *Chem. Sci.* **2017**, *8*, 7923-7931.

[41] E. Bartolami, C. Bouillon, P. Dumy, S. Ulrich, *Chem. Commun.* **2016**, *52*, 4257–4273.

[42] M. Xiong, M. W. Lee, R. A. Mansbach, Z. Song, Y. Bao, R. M. Peek Jr., C. Yao, L.-F. Chen, A. L. Ferguson, G. C. L. Wong, et al., *Proc. Natl. Acad. Sci. U. S. A.* **2015**, *112*, 13155–13160.

[43] Y. Bai, L. Nguyen, Z. Song, S. Peng, J. Lee, N. Zheng, I. Kapoor, L. D. Hagler, K. Cai, J. Cheng, et al., *J. Am. Chem. Soc.* **2016**, *138*, 9498–9507.

[44] N. Zheng, L. Yin, Z. Song, L. Ma, H. Tang, N. P. Gabrielson, H. Lu, J. Cheng, *Biomaterials* **2014**, *35*, 1302–1314.

[45] Y. Hu, B. Xu, Q. Ji, D. Shou, X. Sun, J. Xu, J. Gao, W. Liang, *Biomaterials* **2014**, *35*, 4236–4246.

[46] A. L. Z. Lee, Y. Wang, W.-H. Ye, H. S. Yoon, S. Y. Chan, Y.-Y. Yang, *Biomaterials* **2008**, *29*, 1224–1232.

[47] M. R. El-Aassar, E. E. Hafez, N. M. El-Deeb, M. M. G. Fouda, *Int. J. Biol. Macromol.* **2014**, *69*, 88–94.

[48] L. Dutot, P. Lécorché, F. Burlina, R. Marquant, V. Point, S. Sagan, G. Chassaing, J.-M. Mallet, S. Lavielle, *J. Chem. Biol.* **2010**, *3*, 51–65.

[49] S. Pujals, E. Giralt, *Adv. Drug. Deliv. Rev.* **2008**, *60*, 473–484.

[50] J. M. Priegue, J. Montenegro, J. R. Granja, *Small* **2014**, *10*, 3613–3618.

[51] J. M. Priegue, I. Lostalé-Seijo, D. Crisan, J. R. Granja, F. Fernandez-Trillo, J. Montenegro, *Biomacromolecules* **2018**, acs.biomac.8b00252–12.

[52] J. Reina, A. Rioboo, J. Montenegro, *Synthesis* **2018**, *50*, 831–845.

[53] R. V. Weatherman, L. L. Kiessling, **1996**, *61*, 534–538.

[54] V. J. LiCata, A. J. Wowor, *Methods Cell Biol.* **2008**, *84*, 243–262.

[55] Z. Derewenda, J. Yariv, J. R. Helliwell, A. J. Kalb, E. J. Dodson, M. Z. Papiz, T. Wan, J. Campbell, *EMBO J.* **1989**, *8*, 2189–2193.

[56] I. J. Goldstein, C. M. Reichert, A. Misaki, *Ann. N. Y. Acad. Sci.*, **1974**, *234*, 283–296.

[57] J. H. Naismith, R. A. Field, *J. Biol. Chem.* **1996**, *271*, 972–976.

[58] E. M. Munoz, J. Correa, E. Fernandez-Megia, R. Riguera, *J. Am. Chem. Soc.* **2009**, *131*, 17765–17767.

[59] D. K. Mandal, C. F. Brewer, *Biochemistry* **1993**, *32*, 5116–5120.

[60] J. A. Atem, F. J. Verbeek, E. M. M. Manders, *J Microsc* **1993**, *169*, 375–382.

[61] I. A. Khalil, K. Kogure, H. Akita, H. Harashima, *Pharm. Rev.* **2006**, *58*, 32–45.

[62] S. Vandevyver, L. Dejager, C. Libert, *Traffic* **2012**, *13*, 364–374.

[63] G. Entlicher, J. V. Koštíř, J. Kocourek, *Biochim Biophys Acta (BBA)* **1971**, *29*, 795–797.

[64] F. Duchardt, M. Fotin-Mleczek, H. Schwarz, R. Fischer, R. Brock, *Traffic* **2007**, *8*, 848–866.

Received: ((will be filled in by the editorial staff))
Revised: ((will be filled in by the editorial staff))
Published online: ((will be filled in by the editorial staff))

Supramolecular Membrane Transport Systems

Marisa Juanes[†], *Irene Lostalé-Seijo*[†], *Juan R. Granja*[†] *& Javier Montenegro*[†]*

Supramolecular Recognition and Selective Protein Uptake by Peptide Hybrids

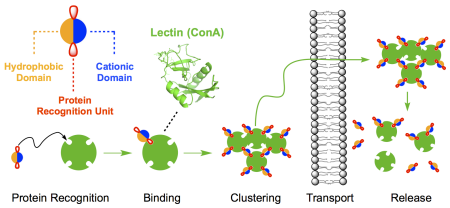

Peptide hybrids are introduced for the selective recognition and translocation of model proteins such as Concanavalin A and Streptavidin.